A&A 383, 697–705 (2002)
DOI: 10.1051/0004-6361:20011734

Astronomy
&
Astrophysics

Magnetic reconnection in 2D stratified atmospheres

II. Observational consequences

I. Roussev[1,2] and K. Galsgaard[3]

[1] High Altitude Observatory, NCAR, 3450 Mitchell Lane, Boulder, CO 80301, USA
[2] Armagh Observatory, College Hill, Armagh, BT61 9DG, N. Ireland
[3] University of St. Andrews, School of Mathematics and Statistics, North Haugh, St. Andrews, Fife, KY16 9SS, Scotland, UK
e-mail: `klaus@mcs.st-and.ac.uk`

Received 1 August 2001 / Accepted 4 December 2001

Abstract. We synthesise three resonance transitions of Li-like ions, C IV 1548.2 Å, O VI 1031.9 Å, and Ne VIII 770.4 Å, based on the MHD experiments presented in Part I of this study. Part I involved 2D MHD modelling of magnetic reconnection events in stratified magneto-hydrostatic atmospheres selected to represent a "quiet" Sun transition region environment. Here in Part II, we discuss some observable consequences of these simulations by including effects of non-equilibrium ionization in a 1D approximation. All spectral line syntheses are done along a particular ray, oriented vertically along the initial current structure. Computed time-series, in the three spectral lines, reveal both blue- and red-shifted Doppler components. It is found to be easier to detect the reconnection event in the various emission lines as strongly Doppler-shifted components as the stratification increases. We predict what the observational consequences of these reconnection events would be, if various spatial resolutions under 1 arcsec become available in future observations. This work is a continuation of previous numerical studies related to solar explosive events.

Key words. MHD – Sun: atmosphere – Sun: transition region – Sun: UV radiation – line: profiles

1. Introduction

Recent studies have presented 2D MHD simulations relevant to the "quiet" Sun explosive events based on magnetic reconnection models (Jin et al. 1996; Innes & Tóth 1999). They suggest the blue- and red-shifted Doppler components observed during explosive events are observational consequences of *bi-directional outflow jets* produced by an ongoing magnetic reconnection. All of these computations, however, involve equilibrium ionization of the emitting plasma. This is an assumption that is unlikely to represent the actual physical situation.

Parallel progress in computing resonance transition region lines under the consideration of *non-equilibrium ionization* was made in the 1D HD simulations of Sarro et al. (1999). This study was aimed at examining changes in the C IV 1548.2 Å transition region line, as a dynamical response to small-scale energy depositions placed at different heights in a 1D coronal loop. The results obtained were (ambitiously perhaps) interpreted as explosive events. Since these simulations involved a different physical mechanism to explain the nature of solar explosive events, the final results were also different, when compared with the 2D reconnection experiments of Jin et al. (1996) and Innes & Tóth (1999). Nevertheless, it has become clear that the consideration of non-equilibrium ionization is a necessary issue in any numerical study aimed at modelling solar explosive events.

In a series of related investigations, Roussev et al. (2001a,b,c,d) explored the dynamical response of various physical conditions, that loosely represent a "quiet" Sun transition region environment, to a magnetic reconnection event. These investigations were intended to model solar explosive events using 2D MHD, and involved model situations ranging from unstratified physical configurations (Roussev et al. 2001a,b,c), to such where the effect of solar gravity was taken into consideration (Galsgaard & Roussev 2002; hereafter referred to as Paper I). It is important to note we did not try to model a realistic solar transition region. Instead, we allowed our flux tubes to have small temperature gradients, and in this way modelling like cool loops. In a recent study based on SUMER observations, Landi et al. (2000) presented new evidence

---

Send offprint requests to: I. Roussev, e-mail: `ilr@ucar.edu` that the emission from the "quiet" Sun transition region (at $T \approx 2 \times 10^5$ K) is dominated by cool loop structures. These are clustered across the network boundaries where solar explosive events tend to occur.

The numerical modelling in our previous studies involved 2D dissipative MHD, including effects of the nonlinear field-aligned thermal conduction, radiative losses, and volumetric heating. Furthermore, time-series in two resonance transition region lines, namely C IV 1548.2 Å and O VI 1031.9 Å, based on the 2D MHD results discussed in Roussev et al. (2001a,b), were computed and presented in Roussev et al. (2001c). These were obtained under the consideration of non-equilibrium ionization (Non-EI) of the emitting plasma. It was found that the observational consequences of reconnection events are strongly dependent on the actual initial physical conditions, though the general dynamics of these events was similar.

The present study is a continuation of Paper I, and is dedicated to examine the observational consequences of the reconnection events discussed there. These studies are more consistent than the ones in Roussev et al. (2001a,b,c), since here the effect of gravity has been taken into account, and thus the models represent a stratified atmosphere. All the computations presented here are based on the MHD experiments discussed in Paper I, and involve the necessary consideration of non-equilibrium ionization (Non-EI). The final results on the line synthesis are presented as time-series in C IV 1548.2 Å, O VI 1031.9 Å, and Ne VIII 770.4 Å, transition region lines, respectively.

As a "blue-print", we first present the set of experiments to be analysed here. This is done in Sect. 2. We then discuss the departures from the equilibrium ionization that are found to take place in the experiments examined in Paper I. Results for this part of our study are summarised in Sect. 3. The line synthesis in the above three spectral lines is presented in Sect. 4, and final conclusions are drawn in Sect. 5.

2. Description of the various experiments

We examine the observational consequences of the reconnection events discussed in Paper I and concentrate on experiments "G1" and "G5". These represent two extreme cases. The most rapid decline of the initial physical quantities with height is exhibited by the "G1" case, while a most gradual decline is present in the "G5". We found significant differences in the dynamics of the magnetic reconnection in the two cases. The main conclusion was that the degree of stratification influences the complexity of the reconnection event, with the strongly stratified physical conditions requiring much longer time to reach a steady state reconnection.

Since the C IV 1548.2 Å, O VI 1031.9 Å, and Ne VIII 770.4 Å, transition region lines, have different temperatures of formation, it proved necessary to perform two additional experiments similar to "G1" and "G5", but at a lower normalised temperature[1], $T_0 = 5 \times 10^4$ K. This highlights the arbitrary choice of the initial conditions that can be made in our exploratory experiments, and in this sense all experiments presented here are ad hoc.

Table 1. Normalisation units in various experiments.

Physical quantity	Notation	G1	G5a	G5b
Length, 10^8 cm	L_0	1.5	1.5	1.5
Alfvén Velocity, 10^7 cm s^{-1}	$V_{\rm A0}$	0.915	0.915	1.293
Time, s	$t_{\rm A0}$	16.4	16.4	11.6
Gravity, 10^4 cm s^{-2}	g_0	2.7	2.7	2.7
Density, 10^{-14} g cm^{-3}	ρ_0	10.04	10.04	5.02
Temperature, 10^5 K	T_0	0.5	0.5	1
End Time, s	$t_{\rm end}$	119	82	49

This paper discusses three of the experiments that have been carried out. The first one refers to experiment "G1" presented in Paper I, where $T_0 = 5 \times 10^4$ K is chosen as the reference temperature. The other two are based on experiment "G5", where T_0 values of 5×10^4 K (experiment "G5a"), and 10^5 K (experiment "G5b") are assigned. A listing of the normalisation units adopted in the three experiments is given in Table 1, including the time in physical units, $t_{\rm end}$, at which each experiment ends.

In order to perform the line synthesis, we choose the line-of-sight to be the jet symmetry axis, $x^* = 0$, along which the maximum flow velocities are reached during the reconnection events. This is vertically along the initial current concentration. We then average the 2D MHD solution over three widths symmetrically across the current sheet. This way, 1D MHD solutions which represent spatial regions of bin-size of 0.1 arcsec ($-0.03 \leq x^* \leq 0.03$), 0.5 arcsec ($-0.12 \leq x^* \leq 0.12$), and 1.0 arcsec ($-0.24 \leq x^* \leq 0.24$) straddling the symmetry axis are obtained. The 1.0 arcsec bin size completely covers the two reconnection jets in the "G5" experiments. The motivation to examine bins of various spatial extents is to determine the observational response if various spatial resolutions of a spectrograph under 1 arcsec are available during observations.

The deriving of the binned data is done using a simple averaging in the horizontal direction. This approach can naturally be questioned as the final result of the analysis are the relative line intensities of the three spectral lines. In observations, the measured intensity represents the emission measure, which is proportional to the line-of-sight integral of the density square for an optical thin line. One could therefore suggest to use a density square weighting of the data instead. A problem with this approach is that we, from a single spectral line, can not deconvolve the intensity information and obtain reliable spatial and temporal information of the physical properties of the emitting plasma. Such information may only be obtained if a full spectrum is simultaneously "inverted".

---

[1] Note this way the normalised value of gravity intensity, g^*, becomes twice higher, since $t_{\rm A0}$ is $\sqrt{2}$ times bigger.

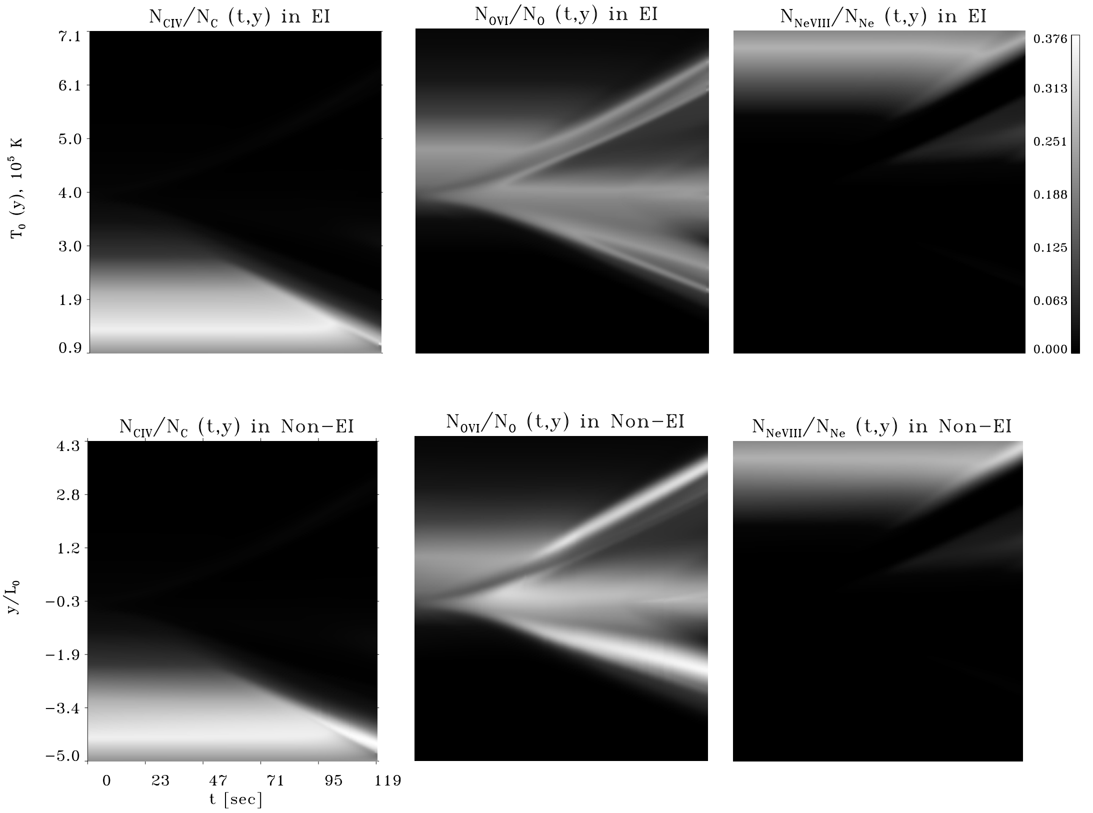

Fig. 1. Images of the relative ion populations of C IV (left), O VI (middle), and Ne VIII (right), as a function of time (from left to right), and position along the line-of-sight (from bottom to top), respectively. The upper panels refer to the case of equilibrium ionization, while the bottom ones correspond to non-equilibrium ionization. These are shown to assess the departures from equilibrium ionization that take place in experiment "G1" using Bin III averaging. The dynamic range of initial temperature (at $t = 0$ s) along the line-of-sight is shown in the upper left panel.

A process that is by no means simple. The approach we have used to derive the spectral information requires knowledge of the physical properties along the line-of-sight to derive the distribution of ions in different states. This information is then integrated along the line-of-sight to produce the actual line profiles, which then includes a density square weighting. Taking this approach, then the simple averaging of the data in the horizontal direction gives the simplest and most sensible weighting of the physical quantities. Therefore, the most appropriate type of averaging one would use to derive various results depends on the approach used to obtain the final result.

3. Departures from equilibrium ionization

As inferred from our previous studies (see Roussev et al. 2001a,c), the assumption of equilibrium ionization (EI) does not apply to the physical conditions involved in the reconnection events examined there. Bulk motions and gradients in the physical conditions produce dynamic time-scales that are short compared to the ionization and recombination times of the emitting plasma[2]. Thus, it is necessary to compute time-dependent ion populations.

The number density, N_i, of a given ion, i, can be obtained by solving the following system of partial differential equations

$$\begin{aligned}\frac{\mathrm{D}\,N_i}{\mathrm{D}\,t} &\equiv \frac{\partial\,N_i}{\partial\,t} + U_x \cdot \frac{\partial N_i}{\partial\,x} + U_y \cdot \frac{\partial N_i}{\partial\,y} \\ &= N_{\mathrm{e}}\left[N_{i-1}\,S_{i-1} + N_{i+1}\left(\alpha_{i+1}^{(\mathrm{r})} + \alpha_{i+1}^{(\mathrm{d})}\right)\right] \\ &\quad -N_{\mathrm{e}}\,N_i\left(S_i + \alpha_i^{(\mathrm{r})} + \alpha_i^{(\mathrm{d})}\right). \qquad (1)\end{aligned}$$

Here $\alpha_i^{(\mathrm{r})}$, $\alpha_i^{(\mathrm{d})}$, and S_i are the rate coefficients of radiative recombination, di-electronic recombination, and collisional ionization for ionization stage i, respectively. Also, U_x, U_y, and N_{e} are the plasma flow velocities and the number density of the electrons, respectively.

A numerical code ("Non-EI" code hereafter) has been developed for the purposes of solving Eq. (1) in 1D, where $|U_x \cdot \partial N_i/\partial\,x| = 0$ by assumption. The ionization and recombination coefficients adopted in this code are those given by Arnaud & Rothenflug (1985). At each time-step, $t = t_j$, all quantities on the right-hand side are known, and Eq. (1) is integrated explicitly to find the solution at a new time-step, $t = t_{j+1}$. The initial populations of oxygen, carbon, and neon used to run the "Non-EI" code are calculated assuming EI. This is consistent with the equilibrium assumptions made for the initial state.

---

[2] The ionization and recombination times for abundant ions in the upper solar atmosphere are typically of the order of ~10–100 s (see Mariska 1992, Sect. 2.4.2)

We examine experiment "G1" (with a bin-size of 1.0 arcsec) which has the longest dynamic time-scales of all our experiments[3]. The relative ion populations $N_{\rm CIV}/N_{\rm C}$, $N_{\rm OVI}/N_{\rm O}$, and $N_{\rm NeVIII}/N_{\rm Ne}$ are shown in Fig. 1, computed from the 1D version of Eq. (1), and in the ionization equilibrium approximation (upper panels). For each ion, relevant images in the two cases are scaled using the same dynamic range. The adjacent grey-scale bar represents the translation table of value versus degree of grey-scale. From bottom to top on each image (along y), the initial temperature (at $t = 0$ s) ranges from 0.87 to 7.11×10^5 K. At the location of the ad hoc diffusion region (placed at $y/L_0 = -0.5$), the temperature is 2.31×10^5 K. Since the temperatures of formation[4] of C IV, O VI, and Ne VIII resonance lines are approximately 1.0, 3.2, and 6.3×10^5 K, respectively, one would expect to encounter an initial situation like that shown in Fig. 1. The peak values of $N_{\rm CIV}/N_{\rm C}$, $N_{\rm OVI}/N_{\rm O}$, and $N_{\rm NeVIII}/N_{\rm Ne}$, are reached at spatial locations $y/L_0 = -4.33$, 0.89, and 3.85, respectively.

By comparing the case of EI with that of Non-EI, one can only see significant differences in C IV and Ne VIII towards the end of the experiment. Departures from EI occur when the contribution from the advective term, $U_y \cdot \partial N_i/\partial y$, becomes comparable or larger than the terms on the right-hand side of Eq. (1). The time-dependent increase of $N_{\rm CIV}/N_{\rm C}$ (respectively $N_{\rm NeVIII}/N_{\rm Ne}$) at a certain y location takes place when the advective term becomes negative. This happens at the expense of C V (respectively Ne IX) which becomes depopulated at that location[5]. In the case of C IV such behaviour is seen after $t \approx 95$ s; while in Ne VIII it happens after $t \approx 80$ s.

As seen in Fig. 1, the largest difference between EI and Non-EI is encountered for the O VI ion. This is expected, since the most rapid changes in the physical conditions are taking place at roughly the formation temperature of the O VI ion. Notice the split of $N_{\rm OVI}/N_{\rm O}$ population into three main branches at $t \approx 30$ s. Two branches appear as double-peaked in EI, and they move farther apart as time passes. As $\partial N_{\rm OVI}/\partial y$ happens to have different signs at the two peaks of each lane, and since U_y does not change its sign, the result is an advective contribution with different signs at the two peaks. In Non-EI, one would therefore expect a time-dependent increase of $N_{\rm OVI}/N_{\rm O}$ at one of the peaks, while the other peak should decrease. This is precisely what Fig. 1 shows. Here the peak population observed at the higher absolute value of y continues to grow in time, while the one at slightly lower y continuously depletes. The increase is found to occur at the expense of O V ion, while the decrease seen in the other peak increases the number distribution of the O VII ion. A similar behaviour is seen in the double-peaked lane of $N_{\rm OVI}/N_{\rm O}$ at negative y positions.

For convenience, let the "blue" jet refer to the one propagating in the positive $y-$direction, while the "red" jet moves in the opposite direction. As seen in Fig. 1, the largest departures from EI occur in the "red" jet, where $N_{\rm OVI}/N_{\rm O}$ also reaches its maximum. Hence, one would expect to see a relatively strong red-shifted Doppler component in the spectra, and a less strong blue-shifted Doppler component. Even some emission at the rest wavelength is expected to be present in the spectra. The "red" jet will be visible in the C IV line, while the "blue" one will be recognised in the Ne VIII line as a blue-shifted Doppler component in the spectra.

It is clear from the discussion so far, that departures from EI indeed take place in the reconnection events presented in Paper I. These affect the various ions differently, with the magnitude of the effect depending on the actual physical conditions encountered. Since we have only analysed experiment "G1" so far, where the dynamical time-scales is longer than in experiments "G5", we infer that deviations from equilibrium values of the three ions will be even larger in the "G5" cases. It has to be mentioned that the analysis made so far applies when the line-of-sight coincides with the jets symmetry axis, along which the maximum flow velocities are reached. We expect to observe smaller departures from EI if there is a slanted angle between the two axes.

4. Line synthesis

4.1. Results from experiment "G1"

Details about the line synthesis algorithm can be found in Roussev et al. (2001a,c). We computed three lines in the three spatial bins of widths 0.1 arcsec (Bin I hereafter), 0.5 arcsec (Bin II), and 1.0 arcsec (Bin III), respectively. The corresponding results are shown in Fig. 2. Instead of showing the line intensity as a function of wavelength, λ, the line profiles are plotted with respect to the Doppler velocity, $v_{\rm D} = c\,(\lambda - \lambda_0)/\lambda_0$, where λ_0 is the rest wavelength. Negative velocities correspond to blue-shifts, while positive values represent red-shifts. The time increases from top to bottom, and thus the last line profile computed in the time-series appears in the foreground. The adjacent image at the top right corner of each surface plot shows the corresponding time-series, $I(\lambda, t)/I_{\rm max}$, in a grey-scale palette. Here $I_{\rm max}$ is the maximum line intensity reached during the whole time-series.

In experiment "G1", it is possible to see the reconnection event in all the three lines. The initial plasma temperature varies along y, as follows: $T = 1.01–4.11$, $0.89–5.66$, and $0.87–7.11 \times 10^5$ K, in Bins I, II and III respectively. At the location of the ad hoc diffusion region the initial temperatures are 1.75, 1.99, and 2.31×10^5 K, respectively. In experiment "G1", the initial temperature gradient along the symmetry axis, $x^* = 0$, is smaller than outside the current concentration (Paper I). Thus, the wider the region

---

[3] We expect even greater departures from EI in experiments "G5".

[4] Here by temperature of formation we mean that, at which the ion responsible for the emission reaches a peak relative population in the case of equilibrium ionization.

[5] This happens since here the advective term is positive.

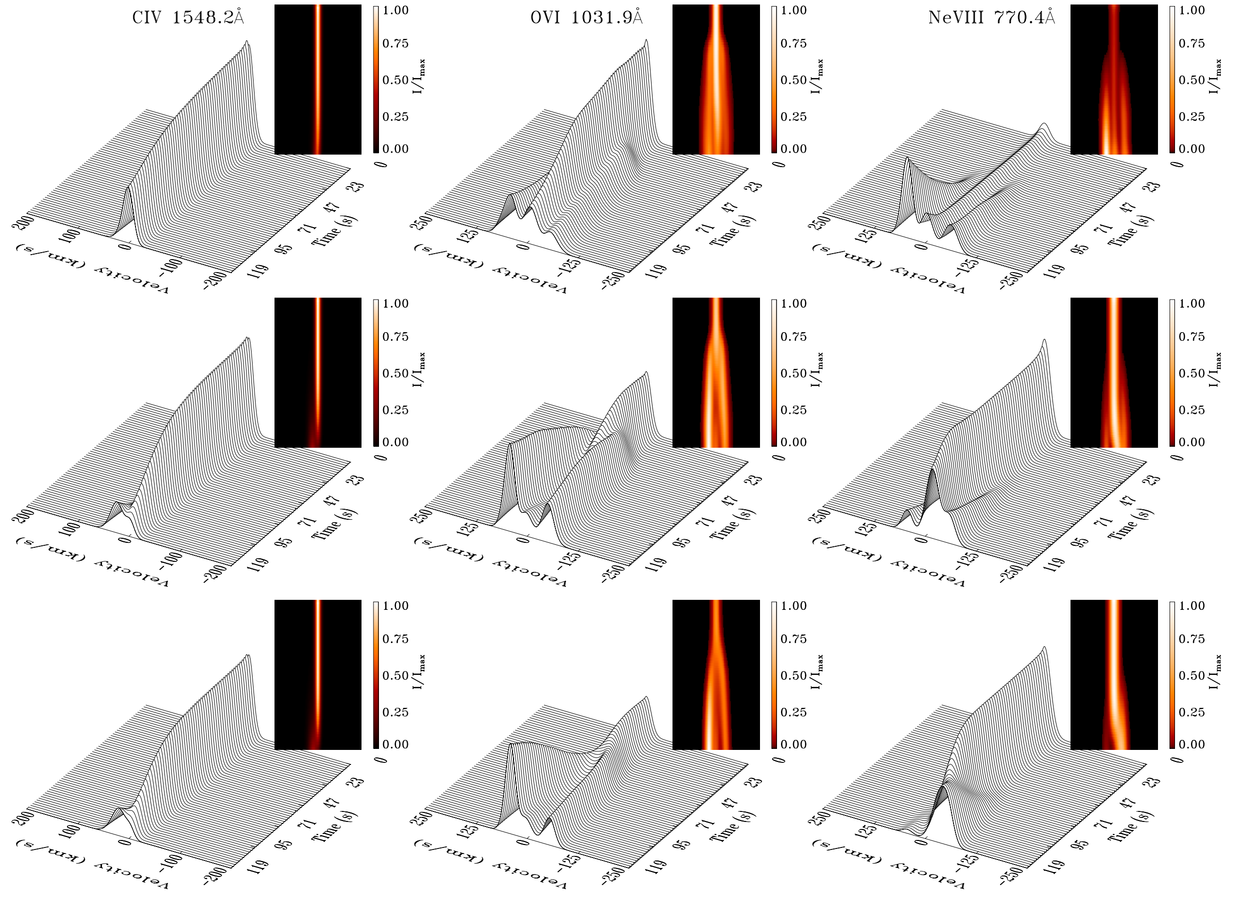

Fig. 2. Line synthesis of experiment "G1" is shown as time-series in C IV λ1548.2 Å (left), O VI λ1031.9 Å (middle), and Ne VIII λ770.4 Å (right), respectively. The results represent the following bins: 0.1 arcsec (top panel), 0.5 arcsec (middle panel), and 1.0 arcsec (bottom panel), respectively. The normalised spectral line intensity, $I(\lambda, t)/I_{\max}$, is shown as a grey-scale image at the top right corner of each surface plot. Notice the time is increasing from top to bottom.

is that we average the temperature over (Bin I–III), the larger the effective variation with height becomes. This has a clear impact on the observable consequences of the reconnection event in the three lines of interest, as seen in Fig. 2.

Since the initial peak population of the C IV ion is obtained far below the reconnection site (see Fig. 1), one does not expect to see any significant changes to the profile of the C IV 1548.2 Å line. In Bin I, this peak population is found very close to the bottom boundary of computational domain. This is why the corresponding time-series (top left in Fig. 2) show no "velocity" events, and reveal only a gradual decrease of the intensity of C IV line with time. In contrast, a slightly red-shifted Doppler component becomes visible in the spectra of Bins II and III towards the end of the experiment (after $t = 90$ s). This is an effect of the temperature in these bins being above the temperature of line formation at the lower boundary of the domain. The plasma parameters in this region are therefore, only being effected as the "red" jet approaches this region of the domain. In the same way, the decrease in the intensity of the central line reflects the change in physical conditions the reconnection jet imposes on this region.

A different physical situation is encountered for the Ne VIII 770.4 Å resonance line. Assuming the initial condition is extended above the numerical domain, then for Bins I and II, the peak population of Ne VIII ion is reached above the top boundary of computational domain, while in Bin III this occurs just inside the top boundary. Although the absolute intensity of the Ne VIII line in Bin I is much lower than in Bin III, the reconnection event is seen in the time-series of Bin I as both red- and blue-shifted Doppler components. The blue component appears at a lower relative intensity, and at a slightly larger velocity than the red component. The presence of the red Doppler component is at first quite surprising. The "red" jet is propagating towards colder and denser plasma and should therefore have much less of a chance to produce a signal in the line profile than the "blue" jet that propagates towards region where the Ne VIII line is formed. By re-scaling the right hand side panels of Fig. 1, it is possible to see a weak presence of the Ne VIII ion at the locations of the "red" jet. Because the density decreases significantly with height, then the density squared effects the line intensity, providing a large signal from the red-shifted Doppler component. In the Bin II time-series, however, the blue-shifted Doppler component is brighter than

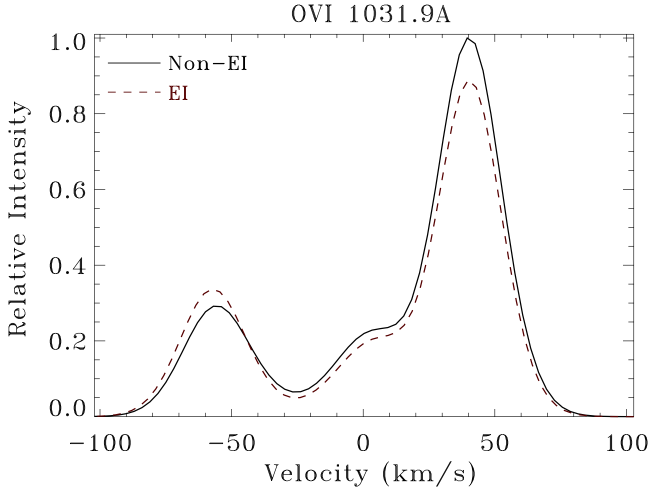

Fig. 3. The line profile of O VI λ1031.9 Å obtained for Bin III of experiment "G1". This is shown at time $t = 119$ s in the case of Non-EI and EI (dashed line).

the red one, and the central line intensity is larger than in Bin I, although the intensity is gradually declining with time. With regard to Bin III, one would expect the "blue" jet to be present as a strong Doppler-shifted component towards the end of the time series. This is confirmed by Fig. 2 (bottom right); the line spectra after $t \approx 90$ s is dominated by this component[6]. The central line intensity rapidly decreases after $t \approx 90$ s, though some finite emission is still present at the end of the time-series. This could be predicted from Fig. 1, where it is seen that the initial region of Ne VIII ions is "pushed" out through the top boundary as the "blue" jet propagates in this direction.

In O VI 1031.9 Å both red- and blue-shifted Doppler components are present in the spectra. This is expected, since the EI peak population in O VI ion is reached inside the computational domain for all three bins. The population peak of Bin III appears closest to the ad hoc diffusion region in the initial physical condition, with the distance to the diffusion region increasing as the spatial resolution of the Bin is increased. Thus, one would observe both the red- and blue-shifted Doppler components as being brighter in the Bin III spectra than in the Bin I profiles. All of this is confirmed by the images in the middle column of Fig. 2. The red-shifted component appears at relatively higher intensity than the blue-shifted in all bins. Toward the end of the time-series, the red- and blue-shifted components both reach approximately the same absolute value of Doppler-shift of about 70 $\mathrm{km\,s^{-1}}$. The maximum Doppler-shift found in the spectra at this time is nearly ± 80 $\mathrm{km\,s^{-1}}$. The line-core intensity centred at rest wavelength is again found to continuously decrease in time, but never reaches a zero intensity. For Bin I, all three emission components have comparable strength, while the Doppler-shifted components dominate in Bin III[7].

Table 2. Summary on the line synthesis relevant to experiment "G1".

Emission Line	C IV 1548.2 Å	O VI 1031.9 Å	Ne VIII 770.4 Å
0.1 arcsec			
I_{λ_0}	1.0^a	8.0×10^{-2}	7×10^{-5}
$I_{\max}/I_{\lambda_0}$	1.10	1.00	5.46
0.5 arcsec			
I_{λ_0}	4.0×10^{-1}	5.0×10^{-2}	4.9×10^{-4}
$I_{\max}/I_{\lambda_0}$	1.04	1.46	1.00
1.0 arcsec			
I_{λ_0}	2.1×10^{-1}	4.0×10^{-2}	7.5×10^{-4}
$I_{\max}/I_{\lambda_0}$	1.04	2.41	1.00

[a] This is given in units of 2.20×10^3 $\mathrm{ergs/(s\,cm^2\,sr\,Å)}$.

Following the discussion made in the previous section, Fig. 3 demonstrates how the departures from EI affect the O VI line profile. This is shown for the case of EI (dashed line) and Non-EI at the final time of the simulation, i.e. $t = 119$ s. It is found that the departures from EI mostly affect the two Doppler-shifted components, with the red one being about 10% brighter in Non-EI than in EI. Here the peak population of O VI in Non-EI nearly coincides with the maximum flow velocity of the "red" jet. In contrast, the blue-shifted component appears at a 5% higher spectral line intensity in EI compared to that in Non-EI. This is because the peak population of O VI in Non-EI is located ahead of the position of maximum flow velocity in the "blue" jet. Furthermore, the line-core intensity is a few % higher in Non-EI than in EI.

The observable consequences of the "G1" reconnection event are different for the various emission lines, as well as the three spatial bins. The corresponding time-series reveal signatures that are similar to those of solar explosive events. The "visibility" of the reconnection jets in the above three lines is well present in the spectra, where they are observed as strongly Doppler-shifted components. A similar picture is revealed during observations of solar explosive events, except for the time-dependent evolution of the line-core intensity (see Teriaca et al. 2001). This could be an indication that most of the intensity in the observations arises from plasma along the line-of-sight that is not involved in the explosive event. This could be investigated by taking different orientations of the line-of-sight, sampling more of the plasma at rest. A summary of the line synthesis made for experiment "G1" is given in Table 2. In this table, I_{λ_0} is the spectral line intensity at the rest wavelength, λ_0, at time zero, where the unit of I_{λ_0} is 2.20×10^3 $\mathrm{ergs/(s\,cm^2\,sr\,Å)}$. The other quantity, $I_{\max}/I_{\lambda_0}$, measures the maximum line intensity reached during the whole time-series in units of I_{λ_0}. From this table, it can be seen that the dominant line, in terms of absolute intensities, is C IV λ1548.2 Å. Less intense is the resonance line of O VI λ1031.9 Å, and the least emission originates from Ne VIII λ770.4 Å. In passing from Bin I to III, I_{λ_0} in C IV and O VI decreases, while it increases

---

[6] It appears at approximately the same value of Doppler-shift as that relevant to Bin II.

[7] This could be inferred from the discussion made above with regard to the O VI ion.

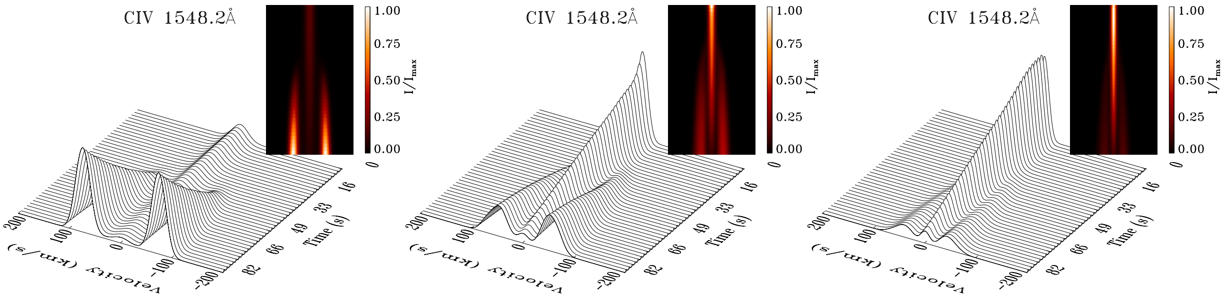

Fig. 4. A set of time-series in C IV λ1548.2 Å relevant to experiment "G5a" is shown. These results refer to spatial bins, as follows, 0.1 arcsec (left), 0.5 arcsec (middle), and 1.0 arcsec (right).

Table 3. Summary on the line synthesis relevant to experiments "G5".

Emission Line	C IV 1548.2 Å	O VI 1031.9 Å	Ne VIII 770.4 Å
Experiment "G5a"			
0.1 arcsec			
I_{λ_0}	9.1×10^{-3}	1.0^a	8.2×10^{-5}
$I_{\max}/I_{\lambda_0}$	10.22	1.21	1.06
0.5 arcsec			
I_{λ_0}	2.8×10^{-1}	3.2×10^{-3}	–
$I_{\max}/I_{\lambda_0}$	1.00	75.76	–
1.0 arcsec			
I_{λ_0}	7.2×10^{-1}	4.9×10^{-6}	–
$I_{\max}/I_{\lambda_0}$	1.05	46343	–
Experiment "G5b"			
0.1 arcsec			
I_{λ_0}	7.2×10^{-3}	4.2×10^{-1}	1.0^b
$I_{\max}/I_{\lambda_0}$	2.31	6.41	1.01

[a] This is given in units of 2.16×10^3 ergs/(s cm^2 sr Å).
[b] Here I_{λ_0} is 6.75×10^1 ergs/(s cm^2 sr Å).

Ne VIII. This is a result of the initial temperature variation between the cold current sheet and the hot exterior, the width of this temperature variations relative the bin size and the formation temperature of the spectral lines.

4.2. Results from experiments "G5"

The initial conditions in experiment "G5" differ from those in the "G1" experiment by having a much larger scale-height. This change has two important effects on the initial conditions of the reconnection experiment in our model. As the scale-height increases, then the variation of the plasma parameters with height decreases, providing a nearly uniform vertical plasma environment. This implies that the horizontal plasma variations across the initial current concentration dominate over the vertical variations. This has naturally significant implications for deriving line profiles, both for the appearance of Doppler profiles in the different spectral lines and also for their observational appearance when different bin sizes are used.

In experiment "G5a", the binned initial plasma temperature varies along y, as follows: $T = 2.85{-}2.91$, $1.45{-}1.51$, and $0.99{-}1.05 \times 10^5$ K, in Bins I, II, and III respectively. At the location of the ad hoc diffusion region, this temperature is 2.88, 1.48, and 1.02×10^5 K, respectively. Because of the small temperature gradient along the line-of-sight, the observational aspects of the magnetic reconnection are mainly limited to a single resonance transition region line. This event is therefore very weak or absent in lines formed at spectral lines with peak intensity at temperatures far away from the plasma temperature of the diffusion region. Table 3 summarises the results for the "G5" experiments in the same format as Table 2. The unit of I_{λ_0} is 2.16×10^3 for experiment "G5a", and 6.75×10^1 ergs/(s cm^2 sr Å) for experiment "G5b", respectively. The Ne VIII λ770.4 Å is very faint for Bin I in experiment "G5a" and has been omitted for the other bins as the relative populations are too low to provide sensible results.

In experiment "G5a" the reconnection event is well observed in C IV λ1548.2 Å. The detailed results are shown in Fig. 4. From left to right in this figure are shown the time-series obtained for Bins I, II, and III, respectively. All plots shown here are prepared in similar manner to those of Fig. 2. In this case, the initial temperature at the ad hoc diffusion region for Bin I, is approximately 3 times higher than the temperature of formation for the C IV line, while the temperature of diffusion region in Bin III is comparable to the formation temperature. The intensity of the initial line will therefore obtain its maximum in Bin III. The resulting time-series in the three Bins reveal the appearance of two almost symmetric Doppler-shifted components at $t \approx 40$ s. The symmetry in this case is caused by the nearly uniform initial temperature along the line-of-sight. The effect of the two jets on the plasma is therefore almost symmetric with regard to the rest wavelength of the spectral line. The line Doppler-shifts reach a maximum value of $\approx \pm 80$ km s^{-1} at the end of computed time-series. The central line intensity is found to decrease with time, and at the end of the time-series, the line intensity of the two Doppler components dominate the spectra.

The O VI λ1031.9 Å line is formed at a temperature that corresponds closely to the temperature of the ad hoc diffusion region in Bin I. From Table 3, it is seen that this

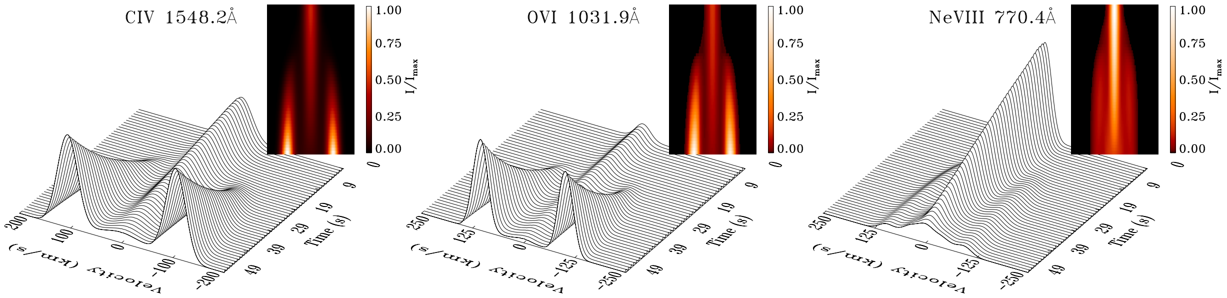

Fig. 5. A set of time-series in C IV λ1548.2 Å (left), O VI λ1031.9 Å (middle), and Ne VIII λ770.4 Å (right), respectively, relevant to experiment "G5b". These results refer to Bin I. Similar to Fig. 3, the normalised spectral line intensity, $I(\lambda, t)/I_{\max}$, is shown as a grey-scale image at the top right corner of each surface plot.

line is the strongest among all three for this experiment, and therefore the easiest to observe. Line profiles derived for the three bins correspond to those shown in Fig. 4 for the C IV spectral line.

Figure 5 shows the appearance of the three spectral lines derived for the "G5b" experiment using the narrow Bin I. This again clearly shows the symmetric appearance of the reconnection jets in the Doppler profiles and the general decay of the line intensity at the rest wavelength. One can also see that the ratio of the rest wavelength to the Doppler components becomes very large for the lines that only have marginal intensity at the rest wavelength.

In this case, the initial plasma temperature varies along y from 6.17 to 6.29×10^5 K, with a temperature at the ad hoc diffusion region of 6.23×10^5 K. One therefore expects that the reconnection event provides the strongest signal in the Ne VIII line that has a formation temperature close to that of the ad hoc diffusion region. This is confirmed by the information provided in Table 3.

At the end of the computed time-series, the two Doppler-shifted components in the three lines have an absolute value of about 110 $\mathrm{km\,s^{-1}}$. A more general discussion of experiments with this characteristic setup can be found in Roussev et al. (2001c).

5. Summary

We have examined the observational consequences of the reconnection events discussed in Paper I, in three resonance transition region lines, namely C IV 1548.2 Å, O VI 1031.9 Å, and Ne VIII 770.4 Å. All computations involved time-dependent ion populations, since departures from the equilibrium ionization were found to take place in the events. This implies that it is necessary to consider *non-equilibrium ionization* in studies of magnetic reconnection events in the solar transition region, when future detailed comparisons between models and observations are to be made.

The line synthesis was based on the data from 2D MHD simulations of magnetic reconnection in a stratified plasma discussed in Paper I. Here experiments with varying degree of stratification were made. By changing the scale-height of the stratification, different characteristics in terms of the structure of the magnetic field and the plasma temperature was achieved. The "G1" experiment represents the case with a short scale-height, which gives a more significant change in the plasma temperature with height than across the current sheet. In the case with a long scale-height, "G5", the dependence on the temperature gradient is reversed and the initial condition becomes increasingly independent of height as the scale-height goes to infinity.

These differences in the initial physical conditions were found to affect the observational consequences of the reconnection events examined in Paper I quite substantially. When the scale-height in the initial physical condition is short, the temperature increase with height makes it possible to observe the reconnection jets in several spectral lines formed at different temperatures. This gives rise to asymmetric line profiles with either the "blue" or the "red" jet dominating the Doppler components in the line spectra. In turn, a large scale-height results in a rather small temperature gradient along the initial current structure, which limits the Doppler signatures to spectral lines with a temperature of formation close to that in the reconnection region. It also changes the appearance of the jets, in that they, will produce nearly identical blue and red Doppler components in the spectral lines in this situation. These changes in the spectral line profiles correspond to those observed during *solar explosive events*.

We examined the observational consequences of reconnection events subject to various spatial resolutions of a spectrograph (under 1 arcsec). For this purpose, we performed line synthesis in the three lines of interest, in regions of various bin-sizes across the line-of-sight, such as 0.1, 0.5, and 1.0 arcsec, respectively. The steeper the gradients in the physical conditions are across the reconnection jets (experiments "G5"), the more substantial are the differences in corresponding spectra of the lines, with the narrow bin showing by far the highest line intensity of the Doppler-shifted components relative to the line-core intensity. The higher the observational resolution, the less of the background plasma at rest is included in the observations, so that the response from the reconnection jets becomes more dominant. Also, when large gradients are present in the plasma across the observational resolution, this will naturally influence the actual observational output away from the physical conditions of the actual jet, i.e., monitoring the intensity at the rest wavelength much better.

The numerical modelling presented here could not reproduce the increase of line-core intensity associated with transient events (see Teriaca et al. 2001). One possible reason for this result is the fact that all computations of time-dependent ion populations used a 1D approximation. In the evolutionary equation, Eq. (1), the advective term associated with the coordinate across the initial current structure, i.e., $|U_x \cdot \partial N_r / \partial x| = 0$, was neglected. A rough estimate of the importance of this term for the O VI ion population in experiment "G1" (see Sect. 3) shows that

$$\left\langle \left\langle \frac{|U_x \cdot \partial N_{\rm OVI} / \partial x|}{|U_y \cdot \partial N_{\rm OVI} / \partial y|} \right\rangle_{(x,y)} \right\rangle_t = 0.12.$$

Here the averaging is first made with respect to the spatial coordinates "$\langle \ \ \rangle_{(x,y)}$", only for $|U_y \cdot \partial N_{\rm OVI} / \partial y| \neq 0$, and then over the whole duration of the experiment "$\langle \ \ \rangle_t$". The maximum value of this ratio without a time-averaging being applied is 0.20. This clearly shows that the 1D approximation used to compute the time-dependent ion species is not completely realistic. Hence, non-equilibrium ionization in 2D must be treated, instead. This will mostly influence the results of the diffusion region and slow-mode shock areas (see Paper I), since these are the locations where the two advective terms are expected to become comparable. Furthermore, all this will affect the results at low absolute values of the Doppler-shifts associated with these regions. This should be taken into consideration in the future, more advanced investigations.

All spectral line syntheses was done along a particular ray, oriented vertically along the initial current structure. This implies that at different slanted angles between the jet symmetry axis and the line-of-sight, the results from the line synthesis will also be different. The results on this aspect of our investigations further confirmed that the observational consequences of these reconnection events are very subtle, clearly dependent on the assumed initial physical conditions and view angle.

Lastly, we emphasize the qualitative means of the numerical results presented in this study. These are required to achieve a better physical interpretation of solar explosive events. Our numerical calculations did not attempt to match any particular set of observations. The physical situations examined here are far too simplistic to do that.

Acknowledgements. The National Center for Atmospheric Research (NCAR) is sponsored by the National Science Foundation. Research at Armagh Observatory is grant-aided by the N. Ireland Dept. of Culture, Arts and Leisure, while partial support for software and hardware is provided by the STARLINK Project which is funded by the UK PPARC. I. Roussev dedicates his studies to Ana and Elena. He is also thankful to the Department of Applied Mathematics, University of St. Andrews, and the NSO in Tucson, Arizona, for the support provided during his visits there. K. Galsgaard was supported by PPARC in a form of Advanced Fellowship, and is thankful for the visitor grant supported by HAO used to initiate this work. The MHD experiments were carried out on the PPARC funded Compaq MHD Cluster in St. Andrews. I. Roussev is grateful to Luca Teriaca for the atomic data provided. We are all very thankful to Tom Bogdan, Phil Judge, Gerry Doyle, B. C. Low, Tom Holzer, and an unknown referee for the useful comments and suggestions made while this manuscript was prepared.

References

Arnaud, M., & Rothenflug, R. 1985, A&AS, 60, 425

Galsgaard, K., & Roussev, I. 2002, A&A, 383, 685

Innes, D. E., & Tóth, G. 1999, Sol. Phys., 185, 127

Jin, S.-P., Inhester, B., & Innes, D. 1996, Sol. Phys., 168, 279

Landi, E., Mason, H. E., Lemaire, P., & Landini, M. 2000, A&A, 357, 743

Mariska, J. T. 1992, The Solar Transition Region (Cambridge University Press, Cambridge)

Roussev, I., Galsgaard, K., Erdélyi, R., & Doyle, J. G. 2001a, A&A, 370, 298

Roussev, I., Galsgaard, K., Erdélyi, R., & Doyle, J. G. 2001b, A&A, 375, 228

Roussev, I., Doyle, J. G., Galsgaard, K., & Erdélyi, R. 2001c, A&A, 380, 719

Sarro, L. M., Erdélyi, R., Doyle, J. G., & Perez, E. P. 1999, A&A, 351, 721

Teriaca, L., Madjarska, M. S., & Doyle, J. G. 2001, Sol. Phys., 200, 91